AD-785 547

THERMAL AND ACOUSTIC FATIGUE OF CERAMICS AND THEIR
EVALUATION

ARMY MATERIALS AND MECHANICS RESEARCH CENTER

PREPARED FOR
ADVANCED RESEARCH PROJECTS AGENCY
ARMY MATERIALS AND MECHANICS RESEARCH CENTER
ARMY MATERIEL COMMAND

JUNE 1974

AD 785 547

REPORT DOCUMENTATION PAGE

READ INSTRUCTIONS
BEFORE COMPLETING FORM

1. REPORT NUMBER	2. GOVT ACCESSION NO.	3. RECIPIENT'S CATALOG NUMBER
AMMRC MS 74-7		

4. TITLE (and Subtitle)	5. TYPE OF REPORT & PERIOD COVERED
THERMAL AND ACOUSTIC FATIGUE OF CERAMICS AND THEIR EVALUATION	June 71 to Sept 73 Final Report
	6. PERFORMING ORG. REPORT NUMBER

7. AUTHOR(s)	8. CONTRACT OR GRANT NUMBER(s)
Charles C. Seaton, 1LT, FA	

9. PERFORMING ORGANIZATION NAME AND ADDRESS	10. PROGRAM ELEMENT, PROJECT, TASK AREA & WORK UNIT NUMBERS
Army Materials and Mechanics Research Center Watertown, Massachusetts 02172 AMXMR-E	ARPA Order Number 2181 AMCMS Code: 5911.21.66022 Agency Accession: DA OE4698

11. CONTROLLING OFFICE NAME AND ADDRESS	12. REPORT DATE
U. S. Army Materiel Command Alexandria, Virginia 22333	June 1974
	13. NUMBER OF PAGES
	33

14. MONITORING AGENCY NAME & ADDRESS(if different from Controlling Office)	15. SECURITY CLASS. (of this report)
	Unclassified
	15a. DECLASSIFICATION/DOWNGRADING SCHEDULE

16. DISTRIBUTION STATEMENT (of this Report)

Approved for public release; distribution unlimited.

17. DISTRIBUTION STATEMENT (of the abstract entered in Block 20, if different from Report)

18. SUPPLEMENTARY NOTES

.

19. KEY WORDS (Continue on reverse side if necessary and identify by block number)

Ceramic materials
Fatigue
Thermal shock
Mechanical properties

Silicon nitride
Silicon carbide
Boron carbide
Titanium diboride

20. ABSTRACT (Continue on reverse side if necessary and identify by block number)

(SEE REVERSE SIDE)

DD FORM 1473 EDITION OF 1 NOV 65 IS OBSOLETE

Block No. 20

ABSTRACT

A brief evaluation of the behavior of some important ceramic materials subjected to thermal and acoustic stress is presented. The criteria for evaluation included measurements of transverse rupture strength, elastic modulus, and internal friction. The chief emphasis is on a brief review of pertinent literature and techniques developed for performing such tests. Comments on the principal results of recent investigations are included. The problem of acoustic fatigue in ceramics was clearly demonstrated. This phenomenon may have important ramifications for the potential use of ceramics in acoustically active environments (e.g., gas turbine blades, bearings, and seals). (Author)
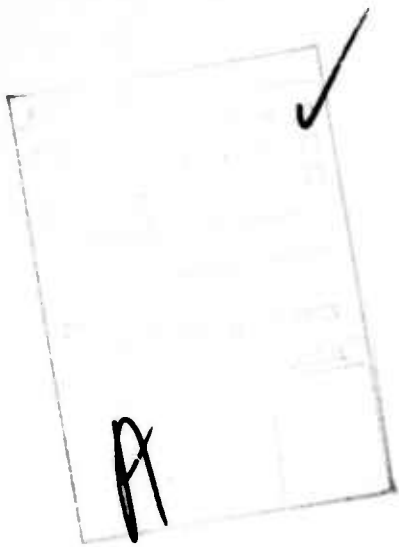
The findings in this report are not to be construed as an official Department of the Army position, unless so designated by other authorized documents.

Mention of any trade names or manufacturers in this report shall not be construed as advertising nor as an official indorsement or approval of such products or companies by the United States Government.

FOREWORD

This report is a summary of investigations performed by the author during the time interval June 1971 to September 1973 under the auspices of the following programs: (1) AMCMS Code Number 501B.11.855, Research in Materials, work unit entitled *X-Ray, Optical, and Mechanical Characteristics of Ceramic Materials* (X.O. 33322); (2) AMCMS Code Number 501A.11.844, In-House Laboratory Independent Research, work unit entitled *Fabrication of Novel Ceramic Base Materials* (X.O. 33301); (3) AMCMS Code Number 502E.11.296, Ceramic Materials Research for Army Materiel, work unit entitled *Synthesis of Boron Compounds* (X.O. 33C07); and (4) ARPA Order Number 2181, AMCMS Code Number 5911.21.66022, work unit entitled *Mechanics of Brittle Materials* (X.O. 32681). All presented data were derived in support of one of the above programs and this report is a compilation demonstrating trends in thermal and acoustic fatigue of ceramics and their evaluation. Details of many of the results and techniques are published elsewhere and will not be repeated in this report.

The author wishes to acknowledge and to express his gratitude to R. N. Katz and C. P. Gazzara for their encouragement and support of these investigations. The cooperation by the Ceramics Research Division staff, particularly J. W. Mc-Cauley and S. K. Dutta is similarly acknowledged, and thanks are due R. F. LaSala for his technical aid in constructing the high-temperature fatigue apparatus.

ib

CONTENTS

ic

NOMENCLATURE

R — Thermal shock parameter useful for predicting resistance to thermal fracture under severe quench, e.g., water quench.

R' — Thermal shock parameter useful for predicting resistance to thermal fracture under mild quench, e.g., air quench.

S — Bend strength measured by four-point loading.

ν — Poisson's ratio.

α — Coefficient of thermal expansion.

k — Thermal conductivity.

E — Young's modulus.

G — Shear modulus.

Q^{-1} — Internal friction.

N — Crack density per unit volume.

m — Mass.

F — First mode of flexural resonant frequency.

F_t — First mode of torsional resonant frequency.

ΔT — Difference between high temperature and quenching medium temperature.

ΔT_c — ΔT just sufficient to cause thermal fracture initiation when quenching into water at room temperature.

T_c — ΔT_c + 25 C (water at room temperature).

ΔT_f — ΔT just sufficient to cause thermal fracture initiation when quenching into any environment.

Δf — Difference between the two frequencies at which the amplitude in a resonant peak defining F is one half the maximum amplitude.

γ — Effective fracture surface energy.

iii

INTRODUCTION

When used as components in applications such as gas turbine engines, ceramics are exposed to an environment which may degrade their structural integrity. Two environmental conditions to which this work was directed were (1) strength deterioration due to thermal stresses (thermal shock) and (2) reduced structural integrity due to low stress oscillations in the kilocycle range (acoustic fatigue). Besides inducing thermal shock and acoustic fatigue conditions on various ceramics, methods of evaluating the effects of these conditions were tested. Whereas measuring strength changes before and after thermal shock or acoustic fatigue is the classical approach to detecting reduced structural integrity, sonic measurements of Young's modulus and internal friction are valuable adjuncts to the former method.

This report is directed toward three major objectives: (1) a literature survey is provided which formed the background for the investigation; (2) experimental techniques used or developed are described; (3) significant results are recorded.

LITERATURE SURVEY

The purpose of this literature survey is to list pertinent references and provide a broad description of the background material forming the basis for the experiments.

Thermal Shock[1-22]

The response of brittle ceramics to thermal shock at a given ΔT depends on the severity of the shock which in turn is dependent upon the quench medium environment. Therefore, it is appropriate to consider two conditions of thermal shock: severe shock, represented by water quenching, and less severe shock, represented by air quenching.

The strength of a ceramic after severe thermal shock is normally constant as the severity of thermal shock ΔT is increased until thermal cracks are nucleated at ΔT_c (Figure 1). An increasing ΔT_c for different ceramics thus corresponds to an increasing resistance to thermal fracture initiation. Kingery,[2] utilizing thermoelastic theory, and Hasselman,[11] following a fracture-mechanical approach, present a thermal shock parameter R which allows one to calculate the relative resistances of ceramics to fracture nucleation undergoing severe thermal shock,

$$\Delta T_c \approx R = \frac{S(1-\nu)}{E\,\alpha}. \tag{1}$$

Although the relationship between ΔT_c and R is not precise, the validity of Equation 1 has been demonstrated; it enables the design engineer to identify those variables which would contribute to an increased ΔT_c.

A second aspect of severe thermal shock which is of particular interest to the design engineer is the extent of damage once ΔT_c has been attained. The fracture-mechanical approach to deriving thermal damage parameters assumes that crack propagation will occur when the strain-energy release rate exceeds the

1
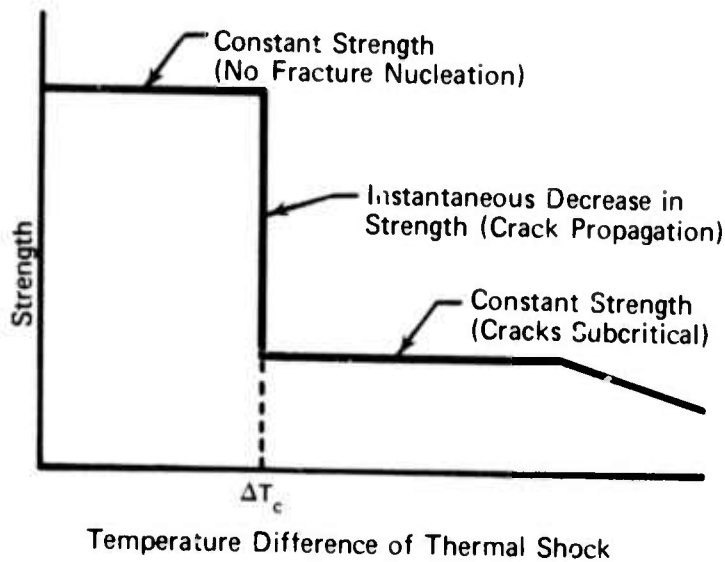
Figure 1. Typical strength behavior of a thermally shocked ceramic. (Ref. 11)

energy required to propagate cracks. Thermal strain energy is thus the driving force and must overcome all mechanisms which dissipate energy during crack propagation. Two parameters have been derived.[5]

$$R''' = [\text{Thermal Strain Energy}]^{-1} = E/(S^2(1-\nu)) \qquad (2)$$

$$\text{and } R'''' = [\text{Effective Fracture Surface Energy}] \; R'''' = E\gamma/(S^2(1-\nu)). \qquad (3)$$

For applications in which thermal fracture cannot be avoided, Equations 2 and 3 may be used as guides for increasing resistance to thermal damage. Possibilities include additions of elastic discontinuities which scatter elastic waves and dissipate energy, increasing porosity which reduces the thermal strain energy available and also increases the effective fracture surface energy, and reducing strength by introducing flaws.

In evaluating the response of brittle ceramics to thermal shock, practical problems arise. The first, locating ΔT_c, is simplified if ceramics have short "critical" cracks prior to thermal shock, where a critical crack is one which controls the macroscopic strength of the specimen. Figure 1 depicts the strength behavior of thermally shocked ceramics having short critical cracks. However, with long critical cracks, strength degradation is not catastrophic but gradual and the location of ΔT_c is more difficult.

Another problem in evaluation is the method of assessing thermal damage. Measuring differences in strength as ΔT is varied yields restricted information since this technique only detects changes in the length of the critical crack. Internal friction, however, measures changes in crack area and thus represents the complete spectrum of cracks, as explained below. Logically, internal friction and R''' or R'''' should correspond closely since the two parameters were derived on the basis of creating surface area, the dimension measured by internal friction. Using strength and internal friction techniques concurrently gives particularly beneficial results; for example, if a microstructure were to allow increased damage via propagation of noncritical cracks rather than critical cracks, this could be readily detected by comparing strength and internal friction data.

2

Whereas the resistance to fracture initiation under severe quenching is governed by one parameter, R, less severe thermal shock is governed by two parameters, R and heat transfer. Thus, a material which is superior to another material in one type of thermal shock test may be inferior in another. Figure 2 depicts differences in ΔT sufficient to cause thermal fracture initiation in a variety of environments, denoted by ΔT_f, as a function of heat transfer. Differences in thermal conductivity among materials will create similar effects. As an example,[1] the resistance to fracture of BeO is superior to Al_2O_3 during air quenching but inferior in the more severe water quench. The reason for this difference is that thermal conductivity is larger for BeO which compensates for a smaller R in an air quench. In the water quench, however, there are no compensating factors for the smaller R so that BeO is less resistant to thermal fracture initiation than Al_2O_3. For mild thermal shock, then, an additional thermal shock parameter is

$$R' = Rk. \tag{4}$$

One other parameter besides R and heat transfer which affects the size of ΔT_f is specimen geometry. This is particularly true for materials in which failure is influenced not only by the maximum stress but also by the distribution of the stress in the material. This is taken into account by the equation

$$\Delta T_f = R' \cdot \frac{1}{r_m h} S, \tag{5}$$
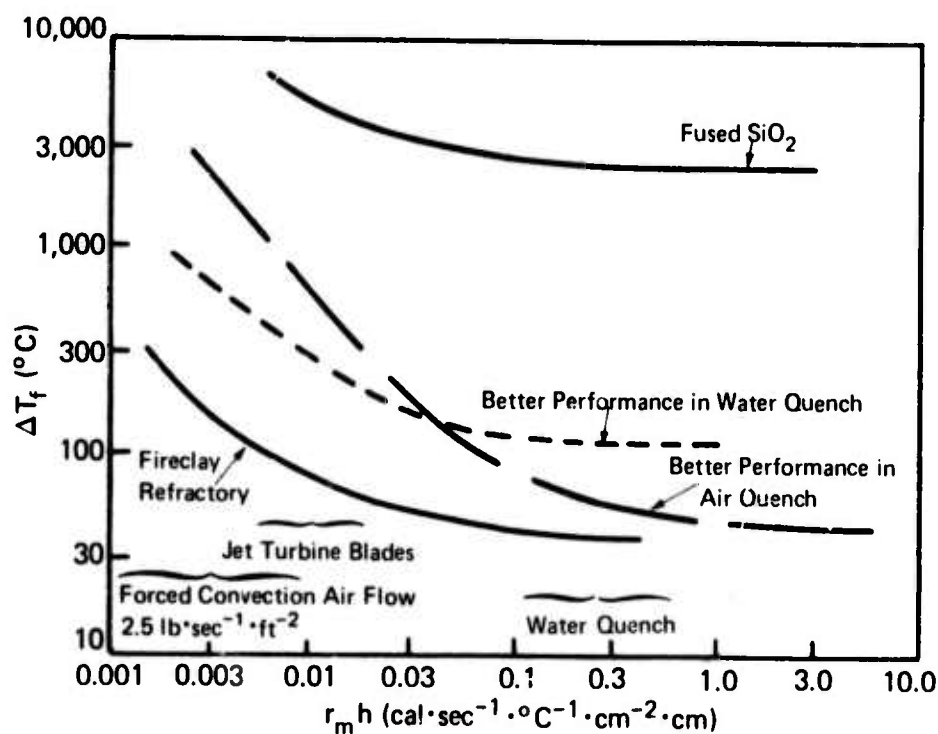
Figure 2. Variation in maximum quenching temperature sufficient to cause fracture initiation (ΔT_f) with different rates of heat transfer ($r_m h$). (Ref. 2)

3

where r_m is a thickness or radial dimension, h is the heat transfer coefficient, and S is a geometric factor. In Figure 2, R', and hence k, is held constant and $r_m h$ is varied. It is apparent that reduced size increases ΔT_f.

Thermal and Mechanical Fatigue[23-29]

Repeated cycles of stress below the fracture strength of a ceramic, whether of thermal or mechanical origin, may cause fatigue. Two approaches to explaining the sources of fatigue have been propounded. (1) A structurally coherent ceramic should survive cyclical stressing indefinitely if the stress level is below the bend strength. Any fatigue effects will be due to growth of pre-existing flaws.[23] (2) Deformation occurring during repeated stressing may be a source of fatigue.[24,28] For example, the generation of lattice defects contributes to cyclic fatigue failure in Al_2O_3. As this cause of fatigue is a thermally activated process, fatigue would be enhanced at higher temperatures, a particularly significant point if such ceramics are exposed to sonic frequency vibrations for extended periods at high temperatures, as in the turbine engine. Both of the above approaches are probably operative and the dominant mechanism of fatigue depends upon whether plastic deformation occurs at the temperature in question.

Sonic Measurements[30-35]

Sonic measurements were used extensively in this program to evaluate the structural integrity of ceramics via measurement of Young's modulus and internal friction.

The following equations relate sonic moduli to the measured resonant frequencies for specimens of rectangular cross sections:

$$E = 0.94645 \frac{CmF^2}{B}, \tag{6}$$

where $C = (D/L)^{-3} [1 = 6.5850 (1 + 0.0752\nu + 0.8109\nu^2) (D/L)^2$

$$- \frac{100.083 (1 + 0.2023\nu + 2.173\nu^2) (D/L)^4}{12 + 76.06 (1 + 14.081\nu + 1.536\nu^2) (D/L)^2} - 0.86806 (D/L)^4];$$

$$G = \frac{4LRmF_t^2}{S}, \tag{7}$$

where $R = \frac{A/B + B/A}{4(A/B) - 2.52 (A/B)^2 + 0.21 (A/B)^6};$

$$\nu = \frac{E-26}{26}, \tag{8}$$

where S is the area of the cross section, R and C are shape factors, A is the length of the smallest dimension, B is the length of the larger dimension, L is the length of the specimen, and D is the dimension of the cross section parallel to the direction of vibration.

From (6), (7), and (8) it may be deduced that the functional relationships between the sonic measurements and mechanical properties are $E = f(F, \nu)$,

4

$G = f(F_t)$, and $\nu = f(E,G)$. F_t may be difficult to determine and E is normally the most important property desired; therefore, assuming $\nu = 0.25$, a value for E may be calculated from the dimensions and F. The assumption of the value for ν is reasonably accurate for most ceramics, and because of the analytical relationship between ν and E small errors in ν would have only a small influence on E.

A ceramic subjected to a stress which damages the microstructure will exhibit in a reduced *Young's modulus.*[36-38] Berry[37] derived the following expression, qualitatively describing this effect,

$$E_{eff} = E_o(1 + 2\pi Nl^2)^{-1}, \tag{9}$$

where E_{eff} = effective E of damaged microstructure, N = crack density, E_o = original E, and l = the crack half-length. As temperature increases, several ceramics have increasing sonic moduli which parallels crack healing.[36-38] Also in accordance with Equation 9, E becomes smaller as ceramics are subjected to increasing thermal shock.

The amplitude of a freely vibrating specimen will decrease with time. The rate of loss of this vibrational energy is termed *damping capacity* or *internal friction*, Q^{-1}. Internal friction is a function of various microscopic and macroscopic processes within the specimen which absorb or dissipate energy.[39-46]

Two methods have been used to measure Q^{-1}. One, the bandwidth method, utilizes the following relationship,

$$Q^{-1} = \frac{\Delta f}{\sqrt{3}F}, \tag{10}$$

where Δf is the difference between the two frequencies at which the amplitude of a vibrating specimen is one half the maximum. A second method involves measuring the time of decay from amplitude A_0 to A_1,

$$Q^{-1} = \frac{1}{F\pi t} \log \frac{A_0}{A_1}, \tag{11}$$

where t is the time interval of decay. From the form of the equations, Equation 10 should be most useful for large values of Q^{-1} and Equation 11 more appropriate for low values of Q^{-1}.

The absorption of acoustic energy may occur by elastic after-effects (relaxation processes) or inelastic deformations (mechanical hysteresis). Significantly, a relaxation process is characterized by having a peak energy absorption at a given temperature and frequency. Examples are point and line defect mobilities, viscous flow, and grain boundary sliding. Mechanical hysteresis, on the other hand, does not exhibit a single relaxation peak; dissipation of energy is relatively independent of temperature and frequency. Line defect mobility and interfacial friction fall within this category. In the following sections each absorption process will be briefly reviewed.

Point Defect Relaxations[47-53]

Defects may respond to externally applied stresses in such a way to cause inelasticity.[47] For instance, the Snoek relaxation in metals is caused by

interstitial impurity movements. Rutile[49] shows a similar behavior. Anion vacancies are another type of point defect which causes relaxation peaks.[48,50,52,53] Another proposed relaxation involves an electronic transition, although this was not substantiated.[51]

Line Defect Relaxations[54-64]

Dislocation behavior of ceramic crystals has been studied by internal friction methods.[54-64] Both relaxation and hysteresis phenomena have been observed, and a complete review of dislocation damping may be found in Burdett and Queen.[62,63] Of the relaxation effects Bordoni[54] first observed while coldworking metals that an internal friction peak, later called the Bordoni peak, increased with coldworking and decreased with annealing. The Bordoni peak occurs at a particular temperature and frequency which is characteristic of a relaxation process. Other dislocation-induced relaxation peaks have since been observed in metals and ceramics. Strain-amplitude-dependent damping, typical of hysteresis effects, occurs at all frequencies and has been related to the movement of dislocation loops over large distances. The hysteresis behavior has been attributed to these loops following different paths during the loading and unloading sequences of the cycle.

Viscous Flow Damping[65]

A viscous material exhibits a relaxation peak which arises from two properties: (1) energy dissipated = relative displacement × shear stress; (2) shear stress = viscosity coefficient × shear stress rate. As temperature increases, displacement also increases due to decreased viscosity, whereas shear stress decreases from the second property above. Since displacement tends to increase and shear stress tends to decrease, the amount of dissipated energy, internal friction, passes through a maximum as temperature is increased. Kerper and Scuderi[65] noted viscous flow relaxation in glasses above the annealing range. Thermally tempered glass did not exhibit viscous flow significantly below the annealing range.

Grain Boundary Slip[66-78]

This process has been extensively studied in ceramics, although little has been done in recent years. Initial research was conducted on metals. Ke[66,67] was the first investigator to identify internal friction behavior at higher temperatures as attributable to grain boundary slip. From his work on metals, he attributed the relaxation peak to the viscous-like behavior of grain boundaries since it had properties similar to viscous flow relaxation. Ke[66] also derived an expression describing the effective grain boundary viscosity.

This theory of grain boundary slip has since been extended to ceramics. The following properties have been observed to change simultaneously with the occurrence of the internal friction relaxation peaks:[77] (1) onset of transient creep; (2) nonlinear variation of Young's modulus with temperature curve; and (3) reduction in strength at high temperatures. Stuart[73] demonstrated the similarity in activation energies between internal friction and transient creep in alumina and observed the coincidence between the temperature of the onset of creep and enhanced internal friction. By implication, relating internal friction to

grain boundary slip should suggest that the above property changes are also a function of grain boundary behavior. Wachtman and Lam[69] and Chang[68,70] did show internal friction to be a function of grain boundary behavior by comparing the energy dissipation of single crystals and polycrystals of alumina. The high temperature internal friction peak was absent from the single crystals. Hanna and Crandall[72] also found a relationship between internal friction magnitude and the mean grain surface area in magnesia at room temperature, suggesting that grain boundary slip might also exist at room temperature. In all of the above cases, the relaxation peak was approximately 1000 C.

Precipitation at grain boundaries of lower viscosity phases enhances grain boundary slipping, as might be expected. BeO^{76} exhibits grain boundary damping which is enhanced by MgF_2 segregation, and $UC_{(1-x)}$ has a much lower temperature relaxation peak than $UC_{(1+x)}$ due to precipitation of uranium metal on the grain boundaries.[78] Additives of Cr_2O_3,[68] and SiO_2[71] to Al_2O_3 have the effect of lowering the temperature at which grain boundary slip occurs.

It has often been reported that two peaks are observed, one usually larger, and occurring at higher temperatures than the other. So far, only the large peak has been considered. An observed smaller peak at lower temperatures is also affected by precipitates.[21,68,75,78] In particular, pure Al_2O_3 does not exhibit the smaller peak, but will if either Cr_2O_3,[68] La_2O_3 or SiO_2[21] is added as an impurity.

Interface Frictional Damping[79-82]

Two faces touching each other and having external shearing forces applied can cause energy losses even though the force may be less than that necessary to cause slippage between the faces. Using this idea, Reid[81] attributed differences in internal friction behavior of fused cast alumina specimens to different intergranular bondings. He likened these grain boundaries to surfaces in contact, but spot welded at various points. Furthermore, he was able to relate both internal friction and strength to the intergranular bondings, which implied that internal friction might be a good nondestructive test for his specimens.

Applications of Internal Friction[21,74,83,84]

From the previous paragraphs it is apparent that the sources of internal friction are dependent on micro- and macrostructural characteristics of the vibrated material. Several areas of study have employed internal friction techniques and will be briefly outlined below.

1. Mechanical fatigue: Schultz and Warwick[83] and DiBeneditto, et al.[84] used internal friction measurements to determine the extent of mechanical fatigue damage in composites. They concluded that the severity of cracking correlated well with the internal friction.

2. Thermal fatigue and shock: Astbury and Davis,[74] in both thermal fatigue and shock, were able to correlate the onset of cracking with drastic changes in internal friction of Al_2O_3. Similar results were obtained with SiC.[21]

3. Polymorphic transformation: Astbury,[80] in examining the internal friction of electrical porcelain as a function of temperature, observed peaks at temperatures corresponding to the α-β quartz transformation. He calculated an activation energy of 30 Kcal/mole which approximates that of alkali-ion diffusion.

4. Porosity effects: Astbury and Davis[74] and Neuber and Wimmer[82] observed internal friction to increase greatly with porosity. Astbury and Davis, in measuring Young's modulus and internal friction as a function of temperature, showed a decrease in the former and an increase in the latter as the amount of porosity was raised.

PERSPECTIVE ON THE UTILITY OF WATER QUENCHING

The purpose of this section is to consider the results of water quenching and how these results relate to other less severe quenching environments, in particular the air quench. Background literature for this discussion is provided in the literature survey.

Differences in behavior among materials undergoing a water quench are due to differences in (1) mechanical properties and (2) geometry. Dissimilarities following an air quench may be traced to (1) mechanical properties, (2) geometry, and (3) heat transfer properties. It follows that the water quench provides a method by which mechanical properties and heat transfer effects may be separated, assuming constant specimen geometry configurations. For example, in developing a material having an improved thermal shock resistance under the air quench, an appropriate starting point is to modify mechanical properties in order to increase its resistance to water quenching. Although a material having increased water quench resistance must have an improved resistance to the air quench, the extent of this improvement is regulated by heat transfer properties. Once the resistance to water quenching has been maximized the heat transfer problems may be pursued. It should be emphasized that it is a mistake to place sole reliance upon the water quench in order to rank various materials under mild shock conditions; test apparatus approximating the environment in which the ceramics are to be used should be the ultimate test.

EXPERIMENTAL PROCEDURES

All thermal shock tests were conducted under water quenching conditions, and this required the construction of a thermal shock apparatus. Specimens were suspended in a vertical-tube, Kanthal-wound furnace by wrapping chromel or alumel thermocouple wire, 0.005 inch in diameter, around each specimen several times. The duration of suspension, always greater than 10 minutes, was determined by the length of time necessary for the temperature equilibration of the system, indicated by a thermocouple resting at the midpoint of the specimen. Water was maintained at room temperature. Before conducting evaluation tests on quenched materials they were first dried thoroughly for at least 24 hours.

High temperature fatigue apparatus was designed and constructed; however, no results were obtained. The critical problem in its future usage is developing a satisfactory temperature distribution in each specimen before air quenching. A detailed description of the apparatus is included in the Appendix.

8

Two methods for evaluating thermal damage were (1) measurement of bend strength and (2) internal friction measurement. Bend strength was determined at room temperature on an Instron testing machine using a crosshead speed of 0.002 inch per minute. The four-point loading fixture had an upper span of 0.25 inch and a lower span of 0.80 inch. Mean strengths and their standard deviations were recorded on 5 to 8 specimens in all cases. The ΔT_c was derived from curves plotting strength versus furnace temperature.

The second method for evaluating thermal damage was by measuring sonic properties[85] E and Q^{-1}. A specimen of rectangular cross section will vibrate in three configurations: (1) flexural, whereby the amplitude of vibration in the first mode resembles a sine wave along the length of the specimen; (2) torsional; and (3) longitudinal. The necessary quantities to be measured were F, the frequency of the first mode of flexural vibration; F_t, the frequency of the first mode of torsional vibration; and Δf, the difference between the frequencies at half amplitude on the resonant curve defining F. These quantities were found using an apparatus* capable of exciting and detecting frequencies up to 25,000 cycles per second. For most geometries, F was within the instrument's range; however, F_t was quite frequently some value in excess of 25,000 cycles per second and thus not subject to measurement.

Two types of transducers were employed. Piezoelectric transducers require the careful positioning of a transducer wire against each end of the specimen, and input and output signals are transmitted through these wires. Piezoelectric transducers enable F and F_t to be measured and allow high temperature measurements. A significant disadvantage to their usage is the occurrence of copious resonant peaks unrelated to the specimen. Electromagnetic transducers were most often used in this work since they do not detect these extraneous peaks and thus the results are more easily interpreted. A major disadvantage of the electromagnetic transducer method is that it does not detect F_t and cannot be used at elevated temperatures. Specimens which are less than 1.5 inches long require the transducers to be in proximity thereby causing interference, and nonmagnetic ceramics require magnetic armatures to be cemented on each end of the specimen.

Because of the complexity of (6), (7), and (8) it was necessary to compose a computer program; a flow chart is included in Figure 3. The program was particularly effective for predicting a range of values in which F_t should be found.

In preparing specimens for sonic analysis, a critical factor is the selection of geometry. In general, both length and mass should be maximized as this increases the accuracy of the test. Dimensions should be parallel and in this study machining dimensions were specified to within ±0.001 inch. Specimens which vibrated with piezoelectric transducers require a roughing of the surface at the point where the transducer wires contact the surface. In applying magnetic armatures to ceramics, shim metal of thickness approximately 0.005 inch was cemented to the ends of each specimen, and each armature weighed of the order of 0.05 grams. A hard fast-drying cement† normally used for attaching strain gages gave satisfactory results. Because of the low total weight of the armatures and cement, there was only a negligible effect on the final measurements of F and Δf.

---

*Magnatest Elastomat Type FM-500, Magnaflux Corp., Chicago, Illinois
†SR-4 Bonding Cement, BLH Electronics, Inc., Waltham, Massachusetts

9
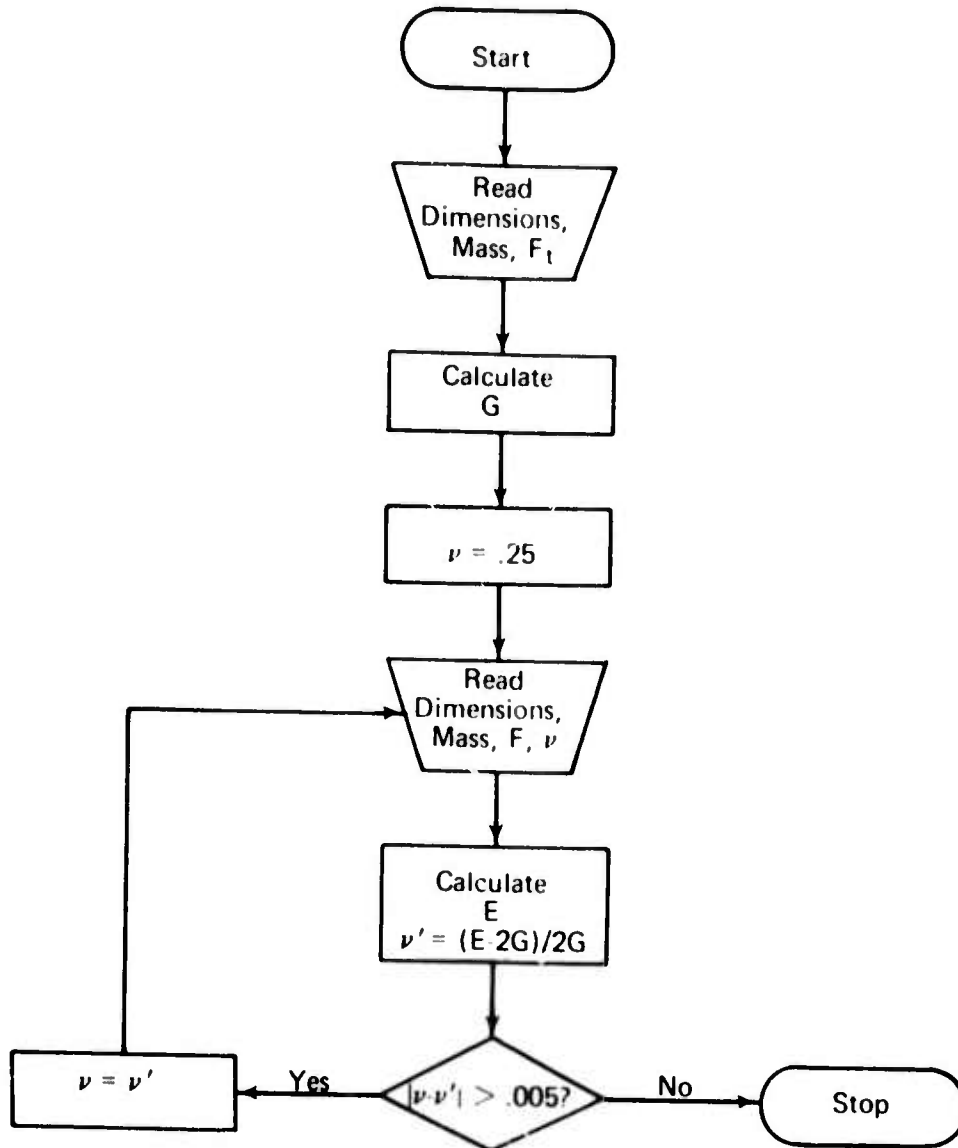
Figure 3. Flow chart of computer program for calculating E, G, and ν.

A final consideration in sample preparation is the method of supporting the specimens. Internal friction of a light specimen is affected in a drastic manner if the support wires are located on a portion of the specimen which has vibration amplitude rather than at a nodal point where there is no amplitude.[86] All internal friction measurements were conducted in the first mode of flexural vibration and the two support wires were located at a distance equal to approximately 0.225 times the total length from each end which corresponds to the nodal points. It should be noted that, contrary to what might be expected, the positioning of the wires had little actual effect on the internal friction measurements. This may have been due to the relatively heavy weight of the specimens, typically three grams or higher. Figure 4 illustrates a setup using electromagnetic transducers.

After many measurements, a standard sequence of events evolved when determining E, G, and ν. (1) Using electromagnetic transducers, F was measured. The first mode and all higher modes of flexural vibration have a Lissajous figure on the oscilloscope trace having the appearance of an ellipse or circle. However, at a frequency approximately one half the first mode of vibration, a figure eight pattern emerges. This was the criterion used in deciding whether a resonant frequency was F or one of the higher modes of vibration. An imperfect or distorted Lissajous figure usually indicates the presence of a perturbation in the system, such as loose armatures. If E was the only property desired, ν was assumed to equal 0.25 and E was computed from the dimensions F and the assumed value of ν. Internal friction was measured employing the bandwidth method because of the large values of internal friction encountered. Thus, Δf was also determined. (2) Using the computer program and the above value for F, F_t was predicted. For ν to be any reasonable value (0.10 to 0.30), where $\nu = f(F, F_t)$, F_t must be confined to values within a range of only a few hundred cycles per second. Since F_t must be determined using piezoelectric transducers, use of the computer program greatly facilitated distinguishing F_t from all other extraneous peaks. (3) After F_t was located, E, G, and ν were recalculated.

Sonic properties at elevated temperatures were also measured, using piezoelectric transducers. Internal friction was measured by the usual bandwidth method. Young's modulus necessitated the use of the following equation,

$$E_T = E_R \frac{F_T^2}{F_R^2 [1 + \alpha(T - T_R)]},$$
(12)

where the subscripts T denote temperature of measurement and T_R room temperature. One difficulty unique to this area of investigation arising from thermal expansion was the necessity to continually readjust the compression on the transducer wires as temperature changed, requiring movement of the transducers by hand.
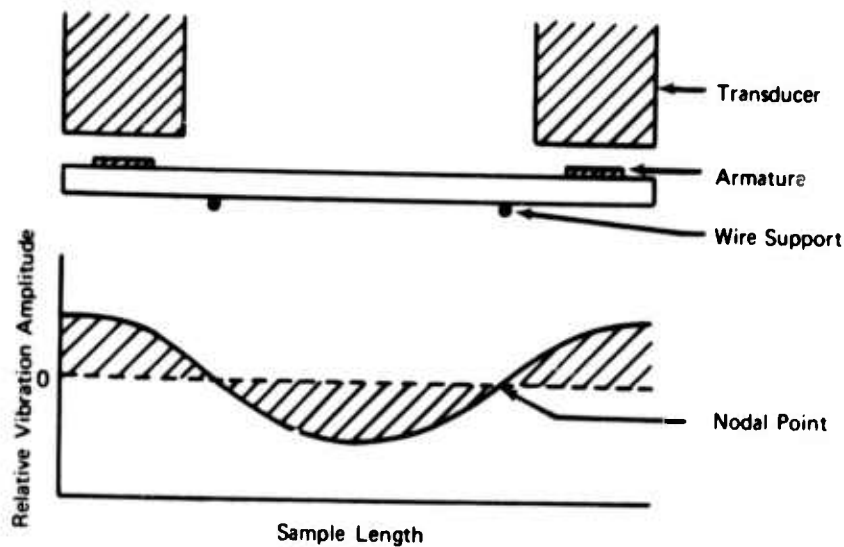
Figure 4. Typical sample setup when using electromagnetic transducers.

SIGNIFICANT RESULTS AND DISCUSSION

Many of the results of this investigation have been or will be published.[87-94] For the material covered elsewhere detailed analysis of the data on which those results are based will not be discussed, although the results will be summarized.

The strength behavior of several boride, carbide, and nitride ceramics after water quenching is represented in Figures 5, 6, and 7. The ΔT_C, denoting the ΔT at which initiation or propagation of the strength-controlling crack occurs, is the most useful parameter derived from these figures and reflects the relative resistances of these ceramics to thermal fracture. Using ΔT_C as the criterion, ten materials were ranked as to increased thermal fracture resistance under conditions of thermal shock into water at room temperature (Table 1). Equation 1 relates the thermal shock parameter R to mechanical properties which should enable an investigator to predict thermal fracture resistance knowing S, E, ν, and α. Table 2 shows the ranking according to R and the mechanical properties used to calculate R. In Figure 8, R and T_c, the furnace temperatures from which the specimens were quenched causing thermal fracture, are compared, and except for B_4C very good agreement exists between R and T_c. Seaton and McCauley[88] concluded that the T_c intercept implies an effective water quench temperature in excess of 100 C. Thus, an important result is that careful control of water temperature is unnecessary when T_c is greater than 200 C.

Seaton and Dutta[89] observed that behavior which indicates a change in thermal crack propagation from a kinetic to quasistatic mode as the average grain size in B_4C was increased from 2 μm to 16 μm. Such a change in behavior may be explained by Hasselman's "Fracture-Mechanical Theory".
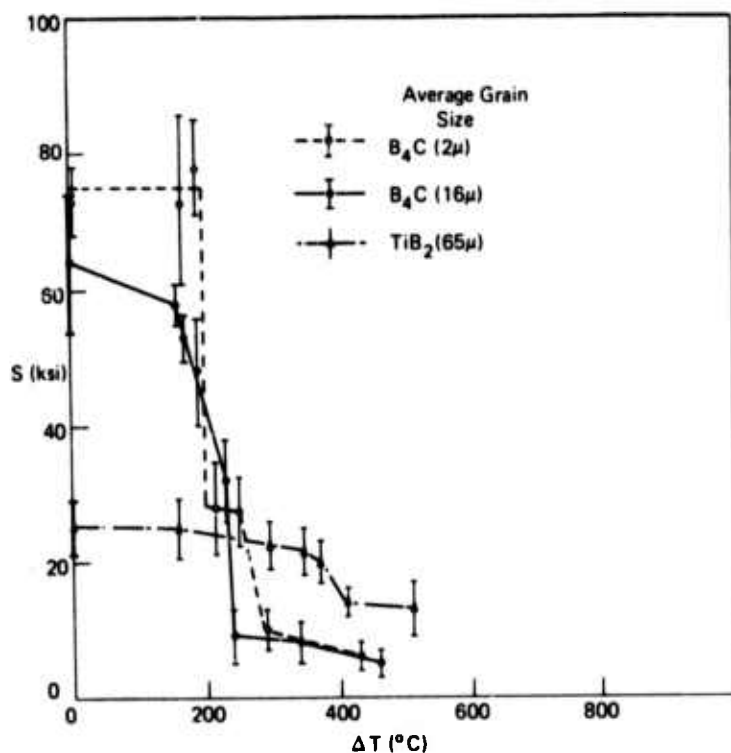
Figure 5. Strength behavior of thermally shocked high boron ceramics.

12

Figure 6. Strength behavior of thermally shocked SiC .
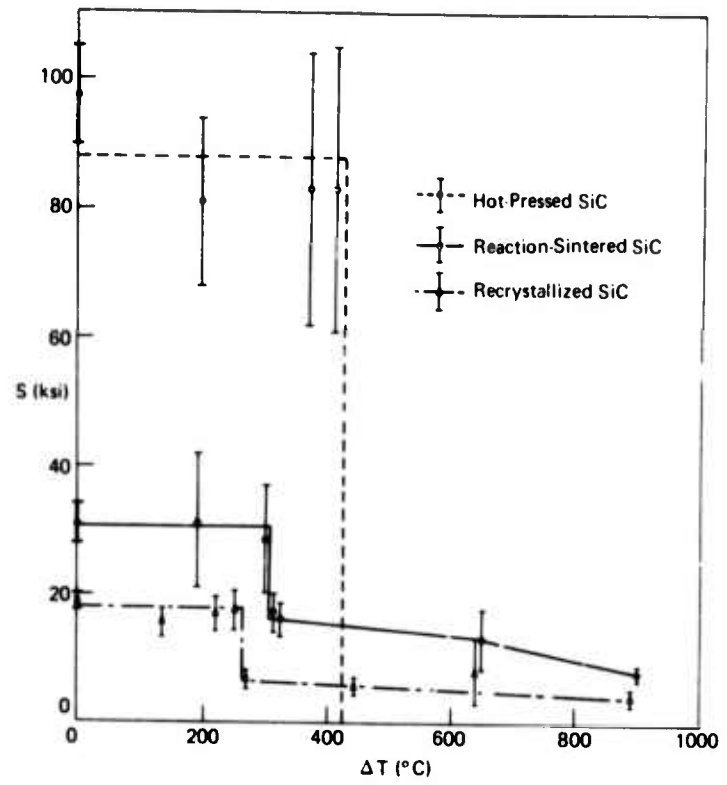
Figure 7. Strength behavior of thermally shocked Si_3N_4.

13
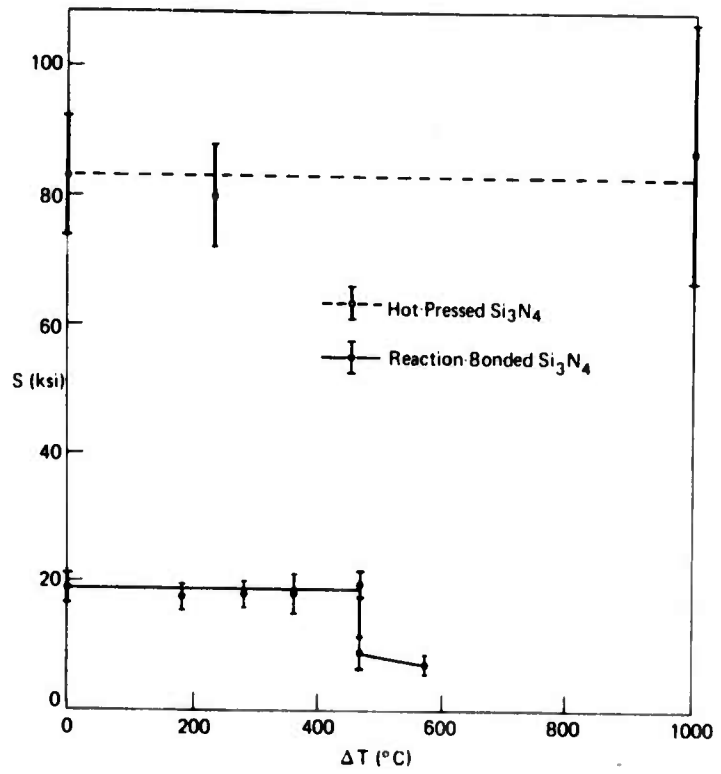
Table 1. RELATIVE RESISTANCES OF VARIOUS CERAMICS TO THERMAL FRACTURE DURING WATER QUENCHING. VALUES OF ΔT_c DERIVED FROM FIGURES 7, 8, AND 9.

Rank	Material*	ΔT_c(°C)	Description
1	B_4C-1	160	Hot Pressed - Avg Grain Size = 16 μm
2	TiB_2	180	Hot Pressed
3	B_4C-2	200	Hot Pressed - Avg Grain Size = 2 μm
4	Al_2O_3†	210	Cold Pressed - Sintered
5	SiC-1	265	Recrystallized
6	Composite†	270	Ba-Mica/Al_2O_3 Composite
7	SiC-2	305	Reaction Sintered
8	SiC-3	415	Hot Pressed
9	Si_3N_4-1	460	Reaction Sintered
10	Si_3N_4-2	>900	Hot Pressed

*Unless otherwise stated dimensions = 0.250" × 0.125" × 2.5"
†Dimensions = 0.125" × 0.100" × 1.5"

Table 2. CALCULATED RESISTANCES OF VARIOUS CERAMICS TO THERMAL FRACTURE UNDER SEVERE QUENCHING

Rank	Material	S_t (10^7) dyne/cm^2	E (10^{10}) dyne/cm^2	ν	α (10^{-6}) (°C^{-1})	R (°C)
1	SiC-1	116.1	236.1	0.14	4.8 (1)	83
2	SiC-2	212.8	359.3	.15	4.0 (2)	126
3	Si_3N_4-1	122.5	125.8	.27	3.2 (1)	222
4	B_4C-1	451.5	410.9	.26	2.4	339
5	B_4C-2	451.5	401.2	.24	2.4	356
6	SiC-3	612.7	416.0	.15	3.4 (3)	368
7	Si_3N_4-2	516.0	297.3	.25	2.8 (4)	465

(1) Alliegro, R. A., and Coes, S. H., ASME 72-GT-20
(2) Estimated
(3) Lange, F. F., ASME 72-GT-56
(4) Torti, M. L., Weaver, C. Q., and Richerson, O. W., ASME 72-GT-19

Internal friction is useful for evaluating thermal shock damage. Data presented by Seaton and Katz[90] showed that some crack growth could be detected below ΔT_c by internal friction measurements. Internal friction and hence total crack area increases rapidly once ΔT_c is exceeded. However, the discontinuity in strength values observed at ΔT_c is not reflected in Q^{-1}.

Seaton and Katz[91] demonstrated the existence of acoustic fatigue at low strain levels in TiB_2. Because strength degradation due to sonic vibration was not accompanied by an increase in internal friction, implying little or no change in crack surface area, a proposed mechanism for acoustic fatigue was the coalescence of microcracks. This idea was confirmed by microscopy which indicated a reduction in the crack density but an increase in the average length of the cracks. This result may have particular relevance in applications such as the turbine engine. If subcritical cracks were formed via thermal fatigue processes the mechanical vibration could conceivably induce acoustic fatigue.

Some interesting but unpublished results concerning high temperature internal friction of TiB_2 provides further information on the anomalous peak alluded to in the literature. The TiB_2, subject to oxidation,[95] was exposed to the ambient atmosphere as internal friction was measured as a function of temperature. Figure 9 shows a well-defined, anomalous internal friction peak beginning at about 500 C. Concurrently, a second glassy phase appears at the grain boundaries in Figure 10. X-ray diffraction patterns were taken of powder samples from the oxidized material in order to analyze the phases present, and TiB_2, TiO_2 (rutile), and a vitreous phase were readily identified. The B_2O_3 was confirmed to be the vitreous phase by quenching hot specimens in water which hydrated the glass. The resulting crystalline phase, $B_2O_3 \times H_2O$, was then identified by X-ray diffraction.

Two possible explanations account for the presence of the anomalous peak. (1) Grain boundary sliding, enhanced by B_2O_3 precipitated at the grain boundaries, commences at approximately 500 C. This temperature is also the melting point of B_2O_3 and helps explain the occurrence of grain boundary sliding at 500 C. However, as the temperature increases, the high vapor pressure of B_2O_3 results in its being vaporized, decreasing the grain boundary sliding. (2) The B_2O_3 promotes an anomalous peak similar to that observed when excess U precipitates on the grain boundaries of UC.[78] Both of the above explanations are plausible, but not enough data exist to distinguish between them. From Figure 9, it is apparent that, because of the shift in the peak with frequency, the anomalous peak is a true relaxation peak supporting either of the two above hypotheses.

A final unpublished result is the dependence of E on temperature for thermally shocked and unshocked Al_2O_3. Young's modulus of Al_2O_3, water quenched from a temperature sufficient to nucleate thermal fracture, initially increases up to 100 C. From that temperature upward E decreases slowly, having a slope similar to that of the unshocked Al_2O_3 (Figure 11). Assuming that the 100 C temperature corresponds to the vaporization of water from the thermal cracks, it is apparent that the presence of water somehow increases the rigidity of the cracked alumina body. This obviously occurs through a transient temperature-dependent mechanism, the nature of which cannot be inferred from the data.
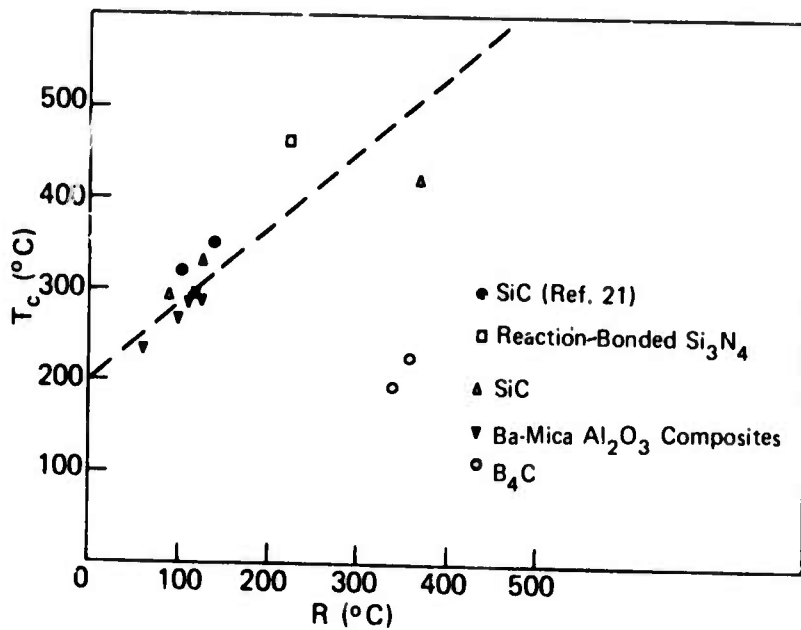
Figure 8. $T_c(^oC)$ versus $R(^oC)$ for various ceramics using data from Tables 1 and 2 unless otherwise indicated.

- ● SiC (Ref. 21)
- □ Reaction-Bonded Si_3N_4
- ▲ SiC
- ▼ Ba-Mica Al_2O_3 Composites
- ○ B_4C

Frequency (T=20 C) = 2890 cps

Frequency (T=20 C) = 3530 cps
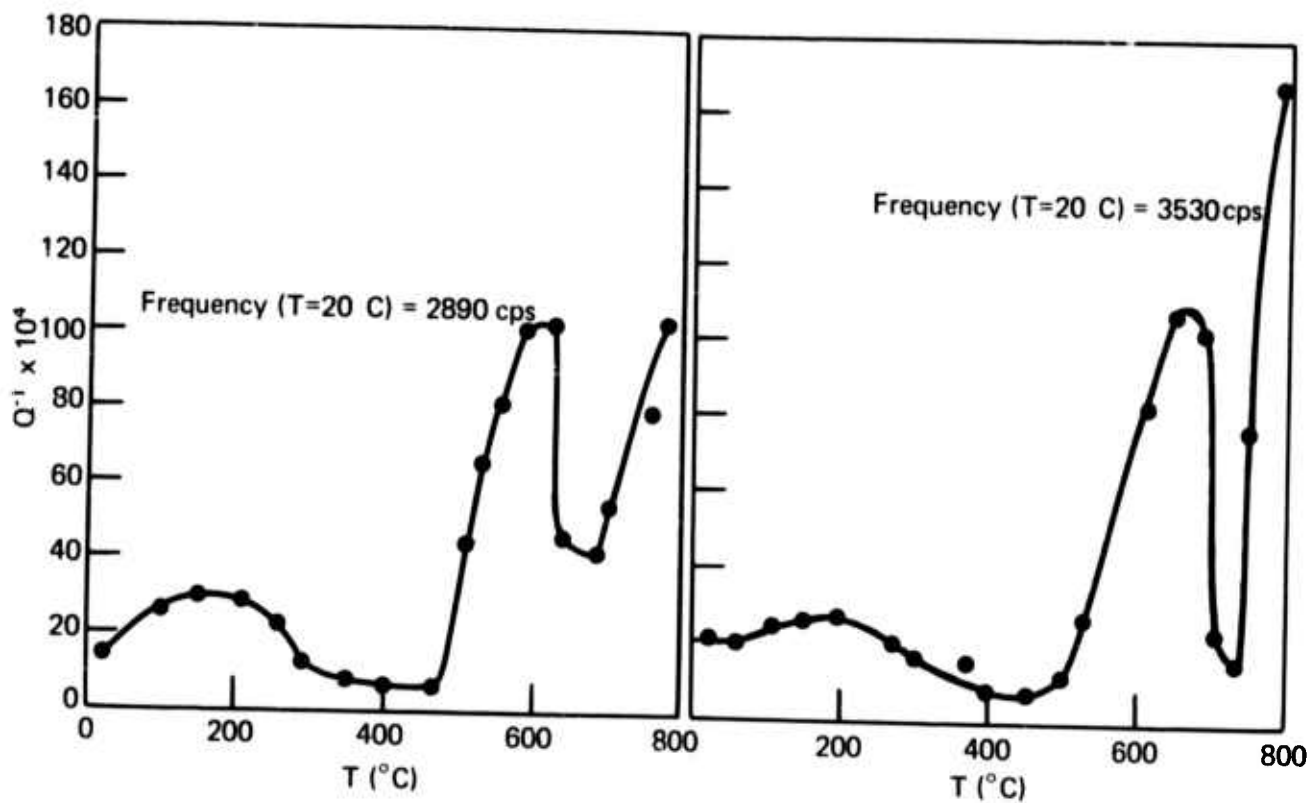
Figure 9. Internal friction of TiB_2 as a function of temperature for two different specimens. The frequency difference between the two samples affected by altering the specimen geometry.

16

Figure 10. TiB$_2$ grain boundary after being heated to 600 C in ambient atmosphere. Mag. 10,000X

Figure 11. Young's modulus of Al$_2$O$_3$, quenched ($\Delta T = 450$ C) and unquenched ($\Delta T = 0$ C) into water, as a function of temperature.

17
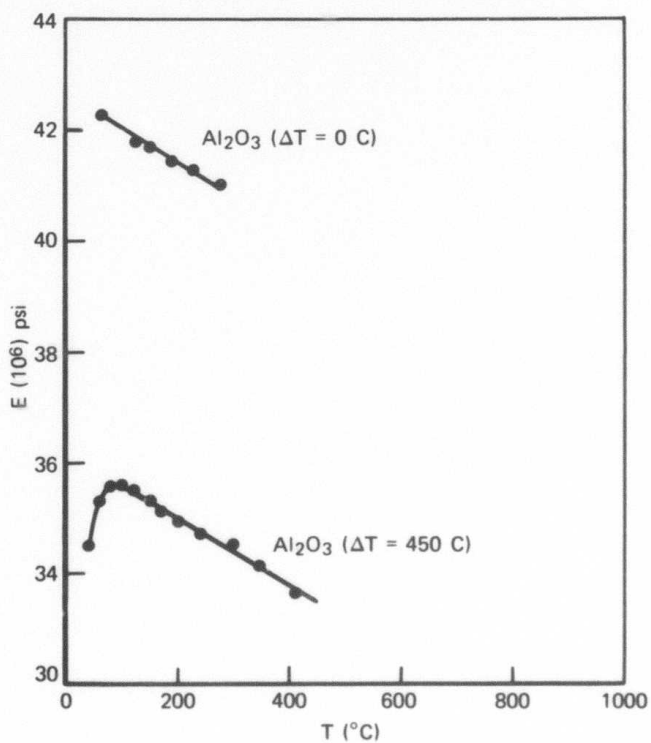
APPENDIX A. THERMAL SHOCK FATIGUE APPARATUS

Thermal shock apparatus for high temperature thermal fatigue tests (Figure A-1), was constructed from an idea originating with Ford Motor Company.[96] The purpose of the thermal fatigue apparatus is to allow the automatic positioning of samples alternately at high temperature and air blast stations. By inserting various timer modules* having different timing scales the investigator may select any time interval at each station. The rotary feed table+ may be adjusted to stop at 4, 6, 12, or 24 stations per revolution of the table, and the counter records the number of cycles up to 100,000. An air manifold allows regulation of the air supply to (1) the rotary feed table and (2) the air nozzle which air quenches the specimens as they are brought from a high temperature station.
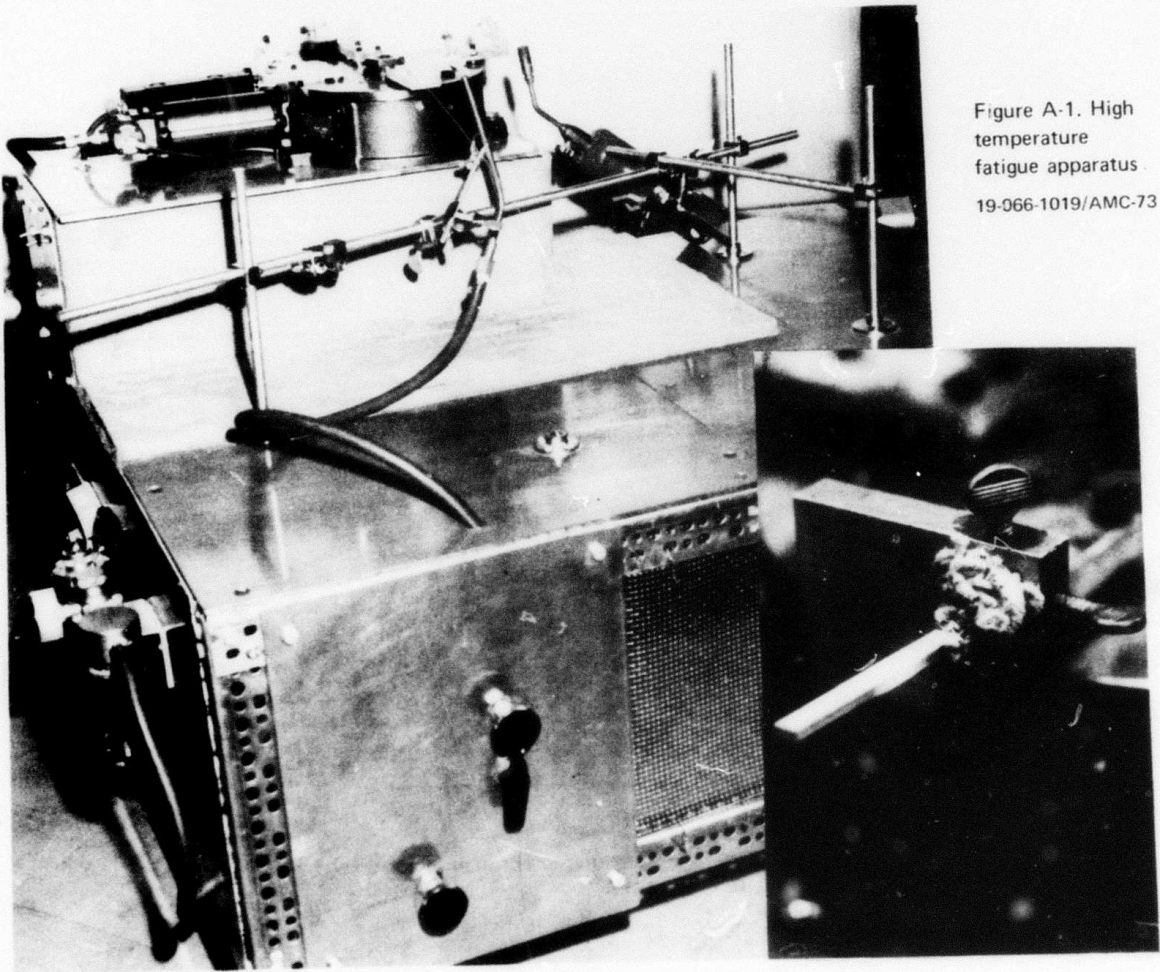
Figure A-1. High temperature fatigue apparatus.

19-066-1019/AMC-73

*HP-5 Series Timer, Eagle Signal, Davenport, Iowa
+Model B3111-003, Bellows Valvair, Akron, Ohio

Preceding page blank

19

The wiring diagram of the high temperature fatigue apparatus is shown in Figure A-2. The timer initiates rotation of the table by activating a delay relay (TR). One function of the relay is to close the circuit between terminals 3 and 4 on the rotary feed table, which energizes the solenoid allowing the table to rotate to the next station. The other function of the relay is to momentarily open the supply current circuit to the timer. This causes the timer to automatically reset the specified time interval required at each station. The orange pilot light identifies switch S_{12} which closes the circuit to the rotary feed table, and the red pilot light denotes switch S_{22} which closes the circuit to the delay relay and timer.
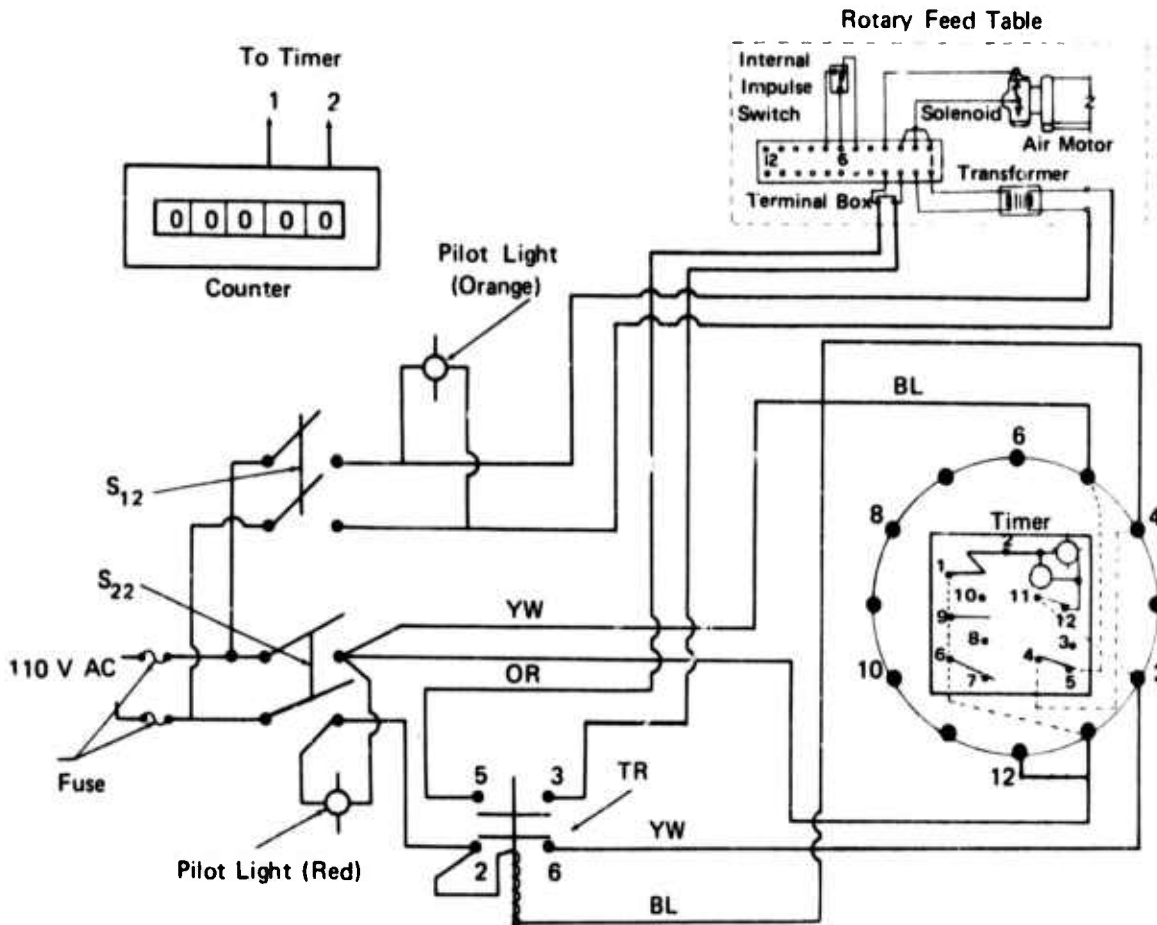
Figure A-2. Electrical wiring diagram of high temperature fatigue apparatus. (drawn by R. F. LaSala)

LITERATURE CITED

1. MANSON, S. S. *Behavior of Materials Under Conditions of Thermal Stress.* NACA TN 2933, 1953.

2. KINGERY, W. O. *Factors Affecting Thermal Stress of Ceramic Materials.* J. Am. Ceram. Soc., v. 38, no. 1, January 1955, p. 3-15.

3. MANSON, S. S., and SMITH, R. W. *Theory of Thermal Shock Resistance of Brittle Materials Based on Weibull's Statistical Theory of Strength.* J. Am. Ceram. Soc., v. 38, no. 1, January 1955, p. 18-27.

4. MANSON, S. S., and SMITH, R. W. *Quantitative Evaluation of Thermal Shock Resistance.* Trans. ASME, v. 4, 1956, p. 533-541.

5. HASSELMAN, D. P. H. *Elastic Energy at Fracture and Surface Energy as Design Criteria for Thermal Shock.* J. Am. Ceram. Soc., v. 46, no. 11, November 1963, p. 535-540.

6. NAKAYAMA, J., and ISHIZUKA, M. *Experimental Evidence for Thermal Shock Damage Resistance.* Bull. Am. Ceram. Soc., v. 45, no. 7, July 1966, p. 666-669.

7. DAVIDGE, R. W., and TAPPIN, G. *Thermal Shock and Fracture in Ceramics.* Trans. Brit. Ceram. Soc., v. 66, no. 8, August 1967, p. 405-422.

8. HASSELMAN, D. P. H. *Approximate Theory of Thermal Stress Resistance of Brittle Ceramics Involving Creep.* J. Am. Ceram. Soc., v. 50, no. 9, September 1967, p. 454-457.

9. HASSELMAN, D. P. H. *Micromechanical Thermal Stresses and Thermal Stress Resistance of Porous Brittle Ceramics.* J. Am. Ceram. Soc., v. 52, no. 4, April 1969, p. 215-216.

10. HASSELMAN, D. P. H. *Griffith Criterion and Thermal Shock Resistance of Single-Phase Versus Multiphase Brittle Ceramics.* J. Am. Ceram. Soc., v. 52, May 1969, p. 288-289.

11. HASSELMAN, D. P. H. *Unified Theory of Thermal Shock Initiation and Crack Propagation in Brittle Ceramics.* J. Am. Ceram. Soc., v. 52, no. 11, November 1969, p. 600-604.

12. AINSWORTH, J. H., and MOORE, R. E. *Fracture Behavior of Thermally Shocked Aluminum Oxide.* J. Am. Ceram. Soc., v. 52, no. 11, November 1969, p. 628-629.

13. HASSELMAN, D. P. H. *Strength Behavior of Polycrystalline Alumina Subjected to Thermal Shock.* J. Am. Ceram. Soc., v. 53, no. 9, September 1970, p. 490-495.

14. HASSELMAN, D. P. H. *Thermal Stress Resistance Parameters for Brittle Ceramics: A Compendium.* Bull. Am. Ceram. Soc., v. 49, no. 12, December 1970, p. 1033-1037.

15. HASSELMAN, D. P. H. *Crack Propagation Under Constant Deformation and Thermal Stress Fracture.* Int. J. of Fract. Mech., v. 7, no. 2, June 1971, p. 157-161.

16. HASSELMAN, D. P. H. *Analogy Between Maximum-Tensile-Stress and Fracture-Mechanical Thermal-Stress-Resistance Parameters for Brittle Ceramics.* J. Am. Ceram. Soc., v. 54, no. 4, April 1971, p. 219.

17. BUESSEM, W. R., and GRUVER, R. M. *Computation of Residual Stress in Quenched Al_2O_3.* J. Am. Ceram. Soc., v. 55, no. 2, February 1972, p. 101-104.

18. GEBAUER, J., KROHN, D. A., and HASSELMAN, D. P. H. *Thermal-Stress Fracture of a Thermomechanically Strengthened Aluminosilicate Ceramic.* J. Am. Ceram. Soc., v. 55, no. 4, April 1972, p. 198-201.

19. GUPTA, T. K. *Strength Degradation and Crack Propagation in Thermally Shocked Al_2O_3.* J. Am. Ceram. Soc., v. 55, no. 5, May 1972, p. 249-253.

20. GUPTA, T. K. *Strength Behavior of Thermally Shocked ZnO.* J. Am. Ceram. Soc., v. 55, no. 8, August 1972, p. 429.

21. COPPOLA, J. A., and BRADT, R. C. *Thermal Shock Damage in SiC.* J. Am. Ceram. Soc., v. 56, no. 4, April 1973, p. 214-216.

22. KROHN, D. A., and HASSELMAN, D. P. H. *Effect of Abrasion and Thermal Stress Resistance of a Soda-Lime-Silica Glass.* J. Am. Ceram. Soc., v. 56, no. 6, June 1973, p. 337-338.

23. KINGERY, W. D. *Thermal Stress Resistance in Property Measurements at High Temperatures.* John Wiley and Sons, 1959, p. 185.

24. WILLIAMS, L. S. *Fatigue and Ceramics.* Mechanical Properties of Engineering Ceramics, W. W. Kriegel and H. Palmour, III, ed., Interscience Publishers, Inc., New York, 1961, p. 245-302.

25. MANSON, S. S. *Thermal Stress and Low-Cycle Fatigue.* McGraw-Hill, Inc., New York, 1966.

26. SARKAR, B. K., and GLINN, T. G. J. *Fatigue Behavior of High-Alumina Ceramics.* Trans. Brit. Ceram. Soc., v. 69, no. 5, May 1970, p. 199-203.

27. BARSON, J. M. *Mechanisms of Corrosion Fatigue Below K_{Iscc}.* Int. J. of Fract. Mech., v. 7, no. 2, June 1971, p. 163-182.

28. KROHN, D. A., and HASSELMAN, D. P. H. *Static and Cyclic Fatigue Behavior of a Polycrystalline Alumina.* J. Am. Ceram. Soc., v. 55, no. 4, April 1972, p. 208-211.

29. WILKINS, B. J. J., and REICH, A. R. *Resistance of Silicon Carbide to Dynamic Fatigue.* Bull. Am. Ceram. Soc., v. 51, no. 5, May 1972, p. 486.

30. PICKETT, G. *Equations for Computing Elastic Constants From Flexural and Torsional Resonant Frequency of Cylinders and Prisms.* Proc. ASTM, v. 45, 1945, p. 846.

31. AULT, N. N., and VELTZ, H. F. G. *Sonic Analysis for Solid Bodies.* J. Am. Ceram. Soc., v. 36, no. 6, June 1953, p. 199-203.

32. SPINNER, S. *Elastic Moduli of Glasses by a Dynamic Method.* J. Am. Ceram. Soc., v. 37, no. 5, May 1954, p. 229-234.

33. WACHTMAN, J. B., and LAM, D. G. *Young's Modulus of Various Refractory Materials as a Function of Temperature.* J. Am. Ceram. Soc., v. 42, no. 5, May 1959, p. 254-262.

34. HASSELMAN, D. P. H. *Tables for the Computation of the Shear Modulus and Young's Modulus of Elasticity From the Resonant Frequencies of Rectangular Prisms.* The Carborundum Company, 1961.

35. DICKSON, R. W., and WACHTMAN, J. B. *An Alumina Standard Reference Material for Resonance Frequency and Dynamic Elastic Moduli Measurement 1. For Use at 25°C.* J. Res. Nat. Bur. Stand., Physics and Chemistry, v. 75A, no. 3, March 1971, p. 155-162.

36. BUSH, E. A. *Influence of Crystal Anisotropy on the Mechanical Properties of Single-Phase Ceramic Materials.* Ph.D. Thesis, Pennsylvania State University, 1958.

37. BERRY, J. P. *Some Kinetic Considerations of the Griffith Criterion for Fracture: I.* J. Mech. Phys. Solids, v. 8, no. 3, March 1960, p. 194-206.

38. BUESSEM, W. R. *Internal Ruptures and Recombinations in Anisotropic Ceramic Materials.* Mechanical Properties of Engineering Ceramics, W. W. Kriegel and H. Palmour, III, ed., Interscience Publishers, Inc., New York, 1961, p. 127-148.

39. ROBERTSON, J. M., and YORGIADAS, A. J. *Internal Friction in Engineering Materials.* Trans. AIME, v. 68, 1946, p. A173-A182.

40. ZENER, F. *Elasticity and Anelasticity of Metals.* University of Chicago Press, Chicago, 1948.

41. LAZAN, B. J. *Effect of Damping Constants and Stress Distribution on the Resonance Response of Members.* Trans. ASME, Ser. E, J. Appl. Mech., v. 75, June 1953, p. 201-209.

42. KNOPOFF, L., and MacDONALD, J. F. *Attenuation of Small Stress Waves in Solids.* Rev. Mod. Phys., v. 30, no. 4, April 1958, p. 1178-1192.

43. STEVENS, R. W. B. *The Applications of Damping Capacity for Investigating the Structure of Solids.* Progr. in Non-Destr. Testing, London, 1958.

44. NIBLETT, D. H., and WILKS, J. *Dislocation Damping in Metals*. Phil. Mag., v. 9, no. 33, 1960, p. 2-89.

45. MARLOWE, M. O., and WILDER, D. R. *Elasticity and Internal Friction Through the Kilocycle Range: Review and Annotated Bibliography*. Iowa State University of Science and Technology, 1964.

46. HUTCHISON, T. S., and BAIRD, D. C. *Physics of Engineering Solids*. John Wiley and Sons, Inc., New York, 1968.

47. BERRY, B. S. *Review of Internal Friction Due to Point Defects*. Acta Met., v. 10, 1962, p. 271-280.

48. WACHTMAN, J. B. *Mechanical and Electrical Resistance in ThO_2 Containing CaO*. Phys. Rev., v. 131, no. 2, February 1963, p. 517-527.

49. CARNAHAN, R. D., and BRITTAIN, J. O. *Point Defect Relaxation in Rutile Single Crystals*. J. Appl. Phys., v. 34, no. 10, October 1963, p. 3095-3104.

50. WACHTMAN, J. B., and CORWIN, W. C. *Internal Friction in ZrO_2 Containing CaO*. J. Res. Nat. Bur. Stand., Physics and Chemistry, v. 69A, no. 5, May 1965, p. 457-460.

51. SOUTHGATE, P. D. *Mechanical Relaxation of a Point Defect in Magnesium Oxide*. J. Appl. Phys., v. 36, no. 9, September 1965, p. 2696-2699.

52. JOHNSON, H. B., TOLAN, M. J., MILLER, G. R., and CUTLER, I. B. *Dipole Relaxation of CaF_2 Doped With NaF*. J. Am. Ceram. Soc., v. 49, no. 8, August 1966, p. 458.

53. LAY, K. W., and WHITMORE, D. H. *Dielectrics and Anelastic Relaxation in Ca-Doped Cerium Dioxide*. Phy. Stat. Sol. (b), v. 43, 1971, p. 175-190.

54. BORDONI, P. G. *Elastic and Anelastic Behavior of Some Metals at Very Low Temperature*. J. Acoust. Soc. Am., v. 26, no. 4, July 1954, p. 495-502.

55. CHANG, R. *Dislocation Relaxation Phenomena in Oxide Crystals*. J. Appl. Phys., v. 32, no. 6, June 1961, p. 1127-1132.

56. HUBER, R. J., BAKER, G. S., and GIBBS, P. *High Temperature Kilocycle Internal Friction in Al_2O_3 Single Crystals*. J. Appl. Phys., v. 32, no. 12, December 1961, p. 2573-2579.

57. BAUER, C. L., and GORDEN, R. B. *Mechanism for Dislocation Pinning in the Alkali Halides*. J. Appl. Phys., v. 33, no. 2, February 1962, p. 672-682.

58. BAKER, G. S. *Dislocation Motion and Damping in LiF*. J. Appl. Phys., v. 33, no. 5, May 1962, p. 1730-1732.

59. DAHLBERG, P., CARNAHAN, R. D., and BRITTAIN, J. O. *Dislocation Damping in Magnesium Oxide Crystals at Low Frequencies*. J. Appl. Phys., v. 33, no. 12, December 1962, p. 3493-3498.

24

60. CARNAHAN, R. D., and BRITTAIN, J. O. *Dislocation Damping in Rutile Single Crystals.* J. Am. Ceram. Soc., v. 49, no. 1, January 1966, p. 15-19.

61. SOUTHGATE, P. D., MENDELSON, K. S., and DePERRO, P. L. *Kilocycle — Range Dislocation Damping in Magnesium Oxide.* Appl. Phys., v. 37, no. 1, January 1966, p. 206-215.

62. BURDETT, C. F., and QUEEN, T. J. *The Role of Dislocations in Damping.* Met. Rev., v. 15, 1970, p. 47-65.

63. BURDETT, C. F., and QUEEN, T. J. *The Role of Dislocations in Damping.* Met. Rev., v. 15, 1970, p. 65-78.

64. BAJONS, P., and WEISS, B. *Internal Friction Studies of Copper After High Frequency Fatigue.* Script. Met., v. 5, 1971, p. 511-514.

65. KERPER, M. J., and SCUDERI, T. G. *Mechanical Properties of Chemically Strengthened Glasses at High Temperatures.* J. Am. Ceram. Soc., v. 49, no. 11, November 1966, p. 613-618.

66. KE, T. S. *Stress Relaxation Across Grain Boundaries in Metals.* Phys. Rev., v. 72, no. 1, January 1947, p. 41.

67. KE, T. S. *Experimental Evidence of the Viscous Behavior of Grain Boundaries in Metals.* Phys. Rev., v. 71, no. 8, August 1947, p. 533-546.

68. CHANG, R. *Creep and Anelastic Studies in Alumina.* USAEC NAAA-SR-2770, 1958.

69. WACHTMAN, J. B., and LAM, D. G. *Young's Modulus of Various Refractory Materials as a Function of Temperature.* J. Am. Ceram. Soc., v. 42, no. 5, May 1959, p. 254-260.

70. CHANG, R. *The Elastic and Anelastic Properties of Refractory Materials for High-Temperature Applications.* Mechanical Properties of Engineering Ceramics, W. W. Kriegel and H. Palmour, III, ed., Interscience Publishers, Inc., New York, 1961, p. 209-220.

71. CRANDALL, W. B., CHUNG, D. H., and GRAY, T. J. *The Mechanical Properties of Ultra-Fine Hot-Pressed Alumina.* Mechanical Properties of Engineering Ceramics, W. W. Kriegel and H. Palmour, III, ed., Interscience Publishers, Inc., New York, 1961, p. 349-379.

72. HANNA, T. J., and CRANDALL, W. B. *Dissipation of Energy at Grain Boundaries.* NASA Doc. N62-11867, 1962.

73. STUART, J. *Internal Friction and Creep in Polycrystalline Alumina.* Tasks 5, IIT Res. Inst., Report Number ASD-TR-61-628 — Part III, 1964.

74. ASTBURY, N. F., and DAVIS, W. R. *Internal Friction in Ceramics.* Trans. Brit. Ceram. Soc., v. 63, no. 1, January 1964, p. 1-19.

75. MARLOWE, M. O., and WILDER, D. R. *Elasticity and Internal Friction of Polycrystalline Yttrium Oxide.* J. Am. Ceram. Soc., v. 48, no. 5, May 1965, p. 227-233.

76. BENTLE, G. G., and KNEIFFEL, R. M. *Brittle and Plastic Behavior of Hot Pressed BeO.* J. Am. Ceram. Soc., v. 48, no. 11, November 1965, p. 570-577.

77. CARNIGLIA, S. C. *Grain Boundary and Surface Influence in Mechanical Behavior of Refractory Oxides — Experimental and Deductive Evidence.* Mater. Sci. Res., v. 3, 1966, p. 425-426.

78. HALL, A. H. *Elastic Moduli and Internal Friction of Some Uranium Ceramics.* J. Nucl. Mater., v. 37, no. 197, 1970, p. 314-323.

79. GOODWIN, L. E., and BROWN, C. B. *Energy Dissipation in Contact Friction: Constant Normal and Cyclic Tangential Loading.* Trans. ASME — J. Appl. Mech., v. 84, March 1962, p. 17-29.

80. ASTBURY, N. F. *II - Some Problems of the Mechanics of Ceramic Materials.* Proc. Brit. Ceram. Soc., no. 6, 1966.

81. REID, D. R. *Mechanical Damping Capacity of Fused Cast Alumina.* Ph.D. Thesis, Rutgers — The State University, 1967.

82. NEUBER, H., and WIMMER, A. *Mechanics of Brittle Materials Under Linear Temperature Increases.* Technical Report AFML-TR-71-70, AD 725761, April 1970.

83. SCHULTZ, A. B., and WARWICK, D. N. *Vibration Response: A Nondestructive Test for Fatigue Crack Damage in Filament-Reinforced Composites.* J. Comp. Mater., v. 5, 1971, p. 394-404.

84. DiBENEDITTO, A. T., GANCHEL, J. V., THOMAS, R. L., and BARLOW, J. W. *Nondestructive Determination of Fatigue Crack Damage in Composites Using Vibration Tests.* J. Mater., v. 7, no. 2, June 1972, p. 211-215.

85. FORSTER, F. *New Method for the Determination of the Modulus of Elasticity and Damping.* Z. Metallk., v. 29, 1937, p. 109 (in German).

86. WACHTMAN, J. B., and TEFFT, W. E. *Effect of Suspension Position on Apparent Values of Internal Friction Determinated by Forster's Method.* Rev. Sci. Instr., v. 29, 1937, p. 109.

87. SEATON, C. C. *A Technique for Determining T_c of Thermally Shocked Ceramics.* Bull. Am. Ceram. Soc., v. 52, no. 12, 1973, p. 897.

88. SEATON, C. C., and McCAULEY, J. W. *Ba-Mica/Alumina Composites: II Thermal Shock Properties.* To be published in the J. Am. Ceram. Soc.

89. SEATON, C. C., and DUTTA, S. K. *Effect of Grain Size on the Crack Propagation of Thermally Shocked Boron Carbide.* J. Am. Ceram. Soc., v. 57, no. 5, 1974, p. 228.

26

90. SEATON, C. C., and KATZ, R. N. *Sonic Degradation of Thermally Shocked Ceramics*. Ultrasonics Symposium Proceedings, Institute of Electrical and Electronics Engineers, Inc., New York, 1972, p. 112.

91. SEATON, C. C., and KATZ, R. N. *Acoustic Fatigue in Certain Ceramic Materials*. J. Am. Ceram. Soc., v. 56, no. 5, May 1973, p. 283.

92. SEATON, C. C., and KATZ, R. N. *Measurement of Internal Friction as a Method for Determining Crack Formation*. Pacific Coast Regional Meeting of Am. Ceram. Soc., Portland, Oregon, 25 October 1972; Bull. Am. Ceram. Soc., v. 51, no. 9, 1972, p. 722.

93. SEATON, C. C. *Internal Friction and Sonic Degradation in Thermally Shocked Ceramics*. New England Section of the Am. Ceram. Soc., Mass. Inst. of Tech., 8 November 1972.

94. KATZ, R. N., SEATON, C. C., and FISHER, E. A. *Thermal Shock Testing of Ceramic Gas Turbine Materials*. Basic Science Ceramic-Metal Systems, Pittsburgh, Penn., 25 September 1973; Bull. Am. Ceram. Soc., v. 52, no. 8, 1973, p. 645.

95. IRVING, R. J., and WORSLEY, I. G. *The Oxidation of Titanium Diboride and Zirconium Diboride at High Temperatures*. J. Less-Comm. Met., v. 16, 1968, p. 103-112.

96. McLEAN, A. F., FISHER, E. A., and BRATTON, R. J. *Brittle Materials Design, High Temperature Gas Turbine*. Contract DAAG 46-71-C-0162, Army Materials and Mechanics Research Center, AMMRC CTR 73-9, March 1973, p. 80.